3rd European supercritical CO2 Conference
September 19-20, 2019, Paris, France

2019-sCO2.eu-148

EXPERIMENTAL INVESTIGATIONS AND SIMULATIONS OF THE CONTROL SYSTEM IN SUPERCRITICAL CO2 LOOP

Ales Vojacek*
Research Centre Řež
Řež, Czech Republic
ales.vojacek@cvrez.cz

Tomas Melichar
Research Centre Řež
Řež, Czech Republic

Petr Hajek
Research Centre Řež
Řež, Czech Republic

Frantisek Doubek
Research Centre Řež
Řež, Czech Republic

Timm Hoppe
XRG Simulation GmbH
Hamburg, Germany

ABSTRACT

An efficient instrumentation and control system (I&C), which is adaptable to loads variations (temperature, pressure, mass flow), is essential for design of power units working with supercritical CO2 (sCO2) to ensure high sCO2 cycle performance with quick response. Hence, sophisticated model-based control system design, supported by dynamic system-level modelling, simulations, and experimental verification is needed. This technical paper presents experimental tests and numerical simulations of the control system of the experimental supercritical CO2 loop at Research Centre Rez (CVR), Czech Republic. The measurements covered testing of temperature, pressure and mass flow controllers. Set-up of the controllers and dynamic response of the system are investigated for several transient scenarios in supercritical and subcritical pressures including transition of the pseudocritical region. The experimental set-up along with the boundary conditions are described in detail, hence the gained data set can be used for benchmarking of system thermal hydraulic codes. Such a benchmarking was performed with the open source Modelica-based code ClaRa using the simulation environment DYMOLA 2019.

INTRODUCTION

The power cycle using sCO2 is an innovative concept which is a competitive alternative to the dominated steam Rankine cycle, gas Brayton cycle or their combination. The sCO2 cycles have a clear potential to attain comparable or even higher cycle efficiencies than conventional steam Rankine/ or Brayton gas cycles [1], [2]. The sCO2 combine many advantages of both the steam Rankine cycle (minimizing the power requirement for compressing the working fluid + heat rejection at low temperatures) and Brayton gas cycle (small size, modular design, fast built units). It also achieves a high degree of thermal recuperation as both Brayton and Rankine cycles. The research activities on sCO2 power plants are progressively increasing during the last decades and there is a growing interest in the worldwide sCO2 events as well. It certainly shows a significant market potential. A report by Sandia Nat. Lab. [3] claims the prospective is to bring the sCO2 cycle to technical readiness level 6 (till 2020) paving the way to demonstration projects (from 2020) and to commercialization (from 2025). The outlook is in line with the testimony of currently running sCO2 projects in Europe, e.g. sCO2-Flex [4].

A number of investigators have carried out extensive experimental tests and analyses of sCO2. However, their work is rather limited to the component behavior studies, i.e. heat transfer and pressure drop models in heaters/coolers/heat exchangers [5], [6], [7]. An exhaustive literature survey on research in supercritical heat transfer is reported in [8]. Very few data can be found on operation and analysis of compressors and turbines [1], [9]-[13]. This is due to the fact that first prototypes of turbomachines are being just built. What is missing is simulation tool which is validated on models of the system level (component interaction) on both steady states and dynamic transients including control system interactions.

The main objective of this work is to provide evidence that the open source Modelica-based code ClaRa [14] is suitable for modeling steady states and transient scenarios along with Proportional Integral Derivative (PID) controllers' actions and their tuning in sCO2 environment. For this purpose, CVR has performed number of experimental tests in the sCO2 facility, located in CVR in the Czech Republic. As a part of experimental campaign, three steady states were selected (covering different temperature levels and pressures) in order to benchmark the numerical model at first place. A set of relevant parameters are given later in the text along with a detailed description of the experimental facility (loop geometry, nominal

DOI: 10.17185/duepublico/48916

pressures, temperatures, heating power and mass flow rate, etc.) to allow preparation of the computational models.

Once the numerical model was cross-checked, the tuning procedure of the PID controllers was performed. There are number of different control loops in the sCO2 loop at CVR. However, as the control mode is most often associated with temperature, hence the temperature controller at the outlet of the heater 2 (H2) was selected to be subject of this work. Many various tuning methods have been proposed from 1942 up to now for gaining better and more acceptable control system response based on our desirable control objectives such as percent of overshoot, integral of absolute value of the error, settling time, manipulated variable behavior and etc. One of the most common PID controller tuning technique used in industry was consolidated and evaluated both from experimental data as well as from the numerical model. The tuning method chosen was the Cohen-Coon method [15] where process dynamics is based on a first order plus deadtime model. The tuning settings was calculated using the Cohen-Coon rules [16] and implemented in both real and Modelica controller. Afterwards, several tests were carried out in order to ensure the response is in line with the overall control objective of the loop.

Above mentioned procedure was conducted for a specific thermal hydraulic condition (pressure, temperature) in the sCO2 experimental loop. For linear processes, where the process characteristics do not change significantly with time or load conditions, then using the set fixed PID parameters will probably be sufficient to ensure effective control. In the case of non-linear processes, however, being limited to a single set of fixed parameters can become problematic. One would need to set the parameters for the worst case, i.e. giving a very low gain, not to cause instabilities in higher gain conditions. In order to find the best overall response, independent sets of PID parameters are needed. Hence, numbers of tests with different conditions were executed with numerical models and different PID sets were derived. Finally, the new sets were implemented in the numerical model and checked for improvements in the control of a process.

The presented results in this paper will benefit to researchers, designers, software engineers, thermal hydraulic specialists, and operators of sCO2 energy systems through the shared measured data in a unique sCO2 facility.

DESCRIPTION OF THE LOOP AND GEOMETRY SPECIFICATIONS

The sCO2 experimental loop at CVR was constructed within SUSEN (Sustainable Energy) project in 2017. This unique facility enables component testing of sCO2 Brayton cycle such as compressor, turbine, HX, valves and to study key aspects of the cycle (heat transfer, erosion, corrosion etc.) with wide range of parameters: temperature up to 550°C, pressure up to 30 MPa and mass flow rate up to 0.35 kg/s. The loop is designed to represent sCO_2 Brayton cycle behavior.

Although the sCO2 loop characteristics are not prototypical of the foreseen sCO2 power plant, the experiments on this simplified facility is sufficient to assess the capability of the numerical codes to deal with the thermal-hydraulic behavior of the sCO2 loop. One of the adaptation of the loop is that a radial compressor expected on the prospective sCO2 power plant is substituted by a piston type pump. In addition, a turbine is replaced by a reduction valve.

Annex A shows the piping and instrumentation diagram (PID) of the loop. The primary circuit is marked in thick red and it consists of following main components:

- The piston-type main pump (MP), which circulates sCO_2 through the circuit with the variable speed drive for the flow rate control.
- The high and low temperature regenerative heat exchangers (HTR HX/LTR HX), which recuperate the heat, hence reduce the heating and cooling power.
- The 4 electric heaters (H1/1, H1/2, H2, H3), which have in total a maximum power of 110 kW and raise the temperature of sCO_2 to the desired test section (TS) inlet temperature up to 550°C.
- The reduction valve which consists of series of orifices to reduce the pressure and together with oil (Marlotherm SH) cooler (CH2) represent a turbine.
- The water cooler (CH1) cools down the sCO_2 at the inlet of the MP by water cooling circuit. The secondary water cooling circuit is cooled by tertiary water cooling circuit. PI&D of the sCO2 loop does not depict tertiary water cooling circuit for simplification matter of the benchmark exercise. The complete sets of boundary conditions are defined for the secondary water cooling circuit allowing this reduced approach.
- Air driven filling (reciprocating) compressor (gas booster station) which pumps the sCO_2 from the CO_2 bottles and also controls the operating pressure.
- Exhaust system for the excess amount of sCO2

The P&ID of the sCO2 loop contains all installed key measurement devices, such as a mass flow meter, Pt-100 sensors, thermocouples, pressure sensors and wattmeters. The nomenclature of the measurement devices respects the KKS identification system for power plants.

The uncertainties provided by the measurement devices, transducer, input card, and control system are summarized in Annex B. The errors correspond to calibration certificates and manufacturer's instructions.

Just for a matter of clarity, the zig-zag line at the P&ID stands for the oil cooler CH2 and connected pipeline. This line was closed during testing campaign since it was not needed to have extra cooling power in oil cooling circuit.

The main operating parameters of the primary circuit are shown in Table 1.

Table 1: The main operating parameters of the sCO2 primary loop.

Maximum operation pressure	25 MPa
Maximum pressure	30 MPa
Maximum operation	550°C

DOI: 10.17185/duepublico/48916

temperature	
Maximum temperature in HTR	450°C
Maximum temperature in LTR	300°C
Nominal mass flow	0.35 kg/s

The sCO2 loop layout is depicted in Figure 1 and the top view of the built facility is shown in Figure 2.

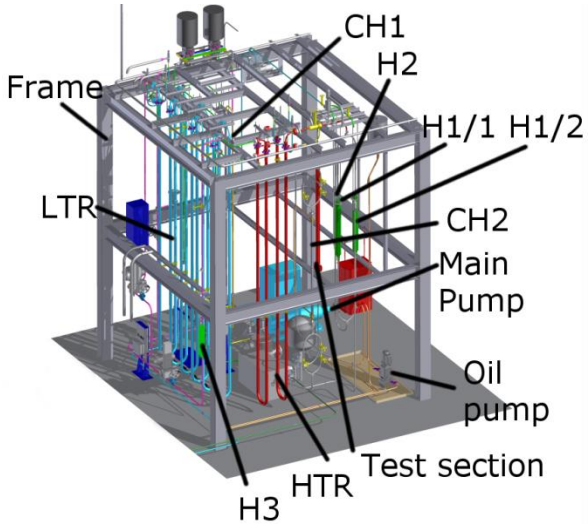

Figure 1: 3D CAD model of the sCO_2 loop.

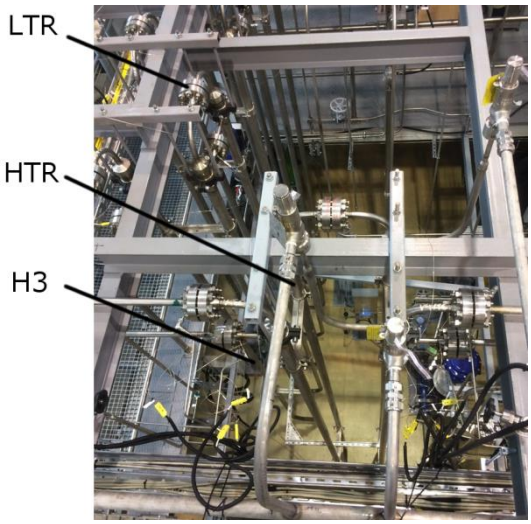

Figure 2: A view from the top on the built sCO_2 loop.

Table 2 summarizes parameters of the MP and the schematic cross-section of the MP is shown in Figure 3.

Table 2: Parameters of the main pump.

Device	**Main Pump - PAX-3-30-18-250-YC-CRYO-drive 9/FM**
Nominal inlet pressure	12.5 MPa
Nominal outlet pressure	25 MPa
Maximal outlet pressure	30 MPa
Nominal inlet temperature	25°C
Maximum inlet temperature	50°C
Nominal isentropic efficiency	0.7
Rotational speed (manufacturer data)	250÷1460 rpm
Volumetric flowrate (manufacturer data)	5÷30 l/min.
Rotational speed -> Volumetric flowrate (measurement data)	555 rpm -> 9.8 l/min 935 rpm -> 16.7 l/min

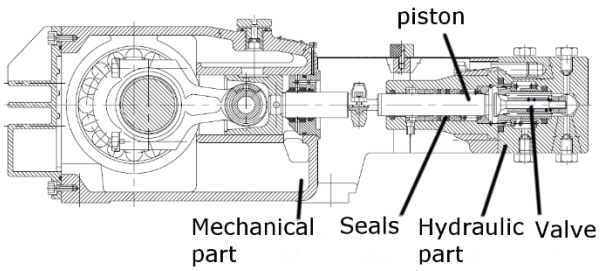

Figure 3: Cross-section of main pump.

In Table 3, the main parameters of the filling compressor are listed.

Table 3: Parameters of the filling compressor.

Device	**Filling compressor - DLE5-15-GG-C**
Nominal inlet pressure of CO_2	0.5 MPa
Nominal outlet pressure	6.5 MPa
Maximum outlet pressure	30 MPa
Nominal flowrate	15 standard litre per minute
Nominal air pressure	0.6 MPa

Geometric parameters of the heat exchanging components of the sCO2 loop needed for preparation of the model are described in

Annex C. The parameters needed for the model settings such as pipe diameters and lengths, layouts of heat exchangers and heaters and materials are listed for each component according to PI&D scheme in the Annex A.

The geometry of HTR heat exchangers is demonstrated in Figure 4. It is a counter-current shell and tube heat exchanger and it concludes of 2 U-tube modules. The LTR heat exchanger is of a same type and it includes 6 U-tube modules.

DOI: 10.17185/duepublico/48916

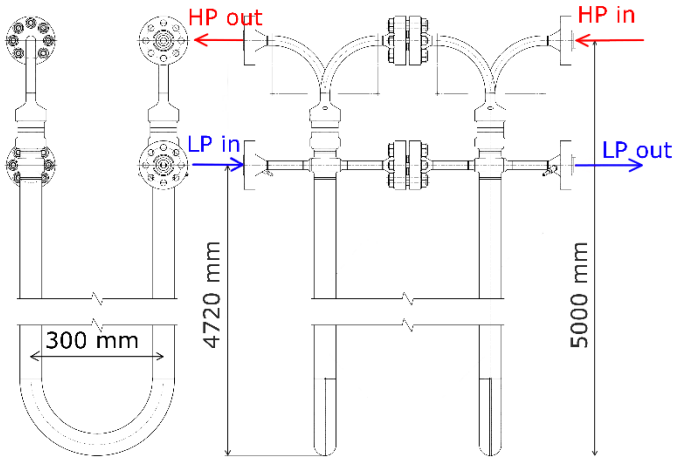

Figure 4: HTR heat exchanger.

The geometry of the tube plate LTR/HTR heat exchanger of inserted in a shell is displayed in Figure 5.

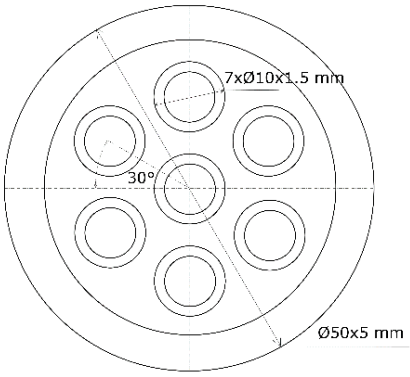

Figure 5: LTR/HTR heat exchanger tube plate in a shell.

The cross cut of electrical heater rod of H1/1, H1/2, H2 and H3 is shown in Figure 6.

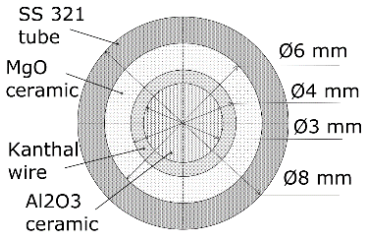

Figure 6: Electrical heater rod cross cut.

The cross cut of electrical heaters of H1/1, H1/2 H3 are shown in Figure 7 and H2 in Figure 8. All heaters are equipped with guiding tube Ø 36 x 2 mm which directs the flow around the electrical heater rods. This tube is plugged on both ends.

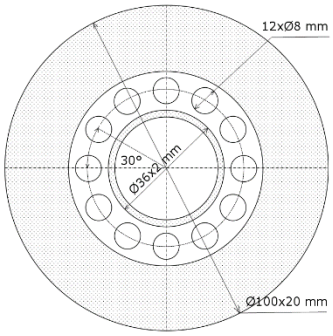

Figure 7: Electrical heater H1/1, H1/2 and H3 cross cut.

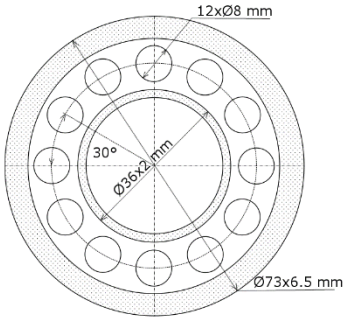

Figure 8: Electrical heater H2 cross cut.

The electrical heater H3 with nominal power 20 kW is positioned at the bypass of the LTR in order to simulate the behavior of a recompression cycle.

The pressure loss coefficients of the valves related to cross-section areas of corresponding pipelines (inner diameter 14 mm) are listed in Table 4.

Table 4: Pressure loss coefficient of the fully-open valves

Valve type	Pressure loss coefficient [-]
Reduction valve (characteristic in Table 5)	827
Control valves (linear characteristic)	14
Closing valves (“hot” part of the loop)	12
Closing valves (“cold” part of the loop)	4

The reduction valve characteristic Opening versus Kv/Kvs of the reduction valve is displayed in Table 5. Averaged values of Kv/Kvs from all measured data covering temperature range 50°C ÷ 450°C are given (no data from manufacturer are available).

Table 5: Characteristic of the of the reduction valve.

Opening [%]	Kv/Kvs [-]
0	0.09
40.5	0.45
45	0.52
50	0.59
55	0.65
60	0.70
65	0.74

DOI: 10.17185/duepublico/48916

70	0.79
75	0.85
80	0.90
85	0.92
90	0.95
95	0.97
100	1.00

The geometric parameters of pipelines according to the PI&D scheme are summarized in Annex D including the pipe diameters and lengths. Parameters of bends are also mentioned to allow modelling of local pressure losses.

The "hot" parts (from inlet to heater H3 and inlet of high pressure LTR to outlet of low pressure LTR) of the loop are insulated with rock wool Orstech DP 100. Thermal conductivity of the insulation material depending on temperature can be found here [17]. The test section and heaters are insulated with 0.14 m thickness and the rest with 0.1 m. is shown in Table 8. The insulation on the RV (of length of approximately 0.5 m) is not installed.

In Annex E, locations of measurement sensors corresponding to the loop layout are listed. The positions of the sensors have to be taken into account in the computational models as well. The table includes all needed sensors of temperature, pressure, mass-flow rate, heating powers and pump speed. Apart from this, positions of valves are also mentioned. Layout of the sensors can be also seen in the PID diagram.

STEADY-STATES BENCHMARK

As a part of the CVR sCO2 loop experimental program for benchmark on thermal hydraulic code, several steady states were achieved. In order to tune the numerical models, 3 selected steady states (covering different temperature levels and pressures) with set of relevant parameters are shown in Annex F along with the results from calculation performed Modelica-based code ClaRa. The simulated results show fair agreement, demonstrating reasonable accuracy of the simulation tool. There are maximum 2.5 K/0.2 MPa/0.6 kW temperature/pressure/heating power errors respectively.

DESIGN OF A NUMERICAL MODEL IN THE CLARA LIBRARY

The performance of the sCO2 loop CVR is simulated with a numerical model, developed in the Modelica language within Dymola environment, using the free ClaRa library.

Modelica

Modelica is a specialized object-oriented equation-based language for physical modelling. Nowadays it is widely used in industry and research for object oriented modelling and transient simulation of cyber physical systems. It is designed for simulation of complex multi-domain systems, e.g., systems containing mechanical, electrical, electronic, hydraulic, thermal, control, electric power or process-oriented subcomponents [18]. The Modelica language is based on equations and thus, on the contrary to the block-oriented languages (e.g. Simulink), the exact computational strategy is left to the tool itself in the compilation phase. This approach allows us to combine components (predefined or custom-built) using connectors and leave the derivation of computation causality to the machines [19]. From the authors' experience, this not only significantly saves time, but helps to avoid a number of mistakes and enables component reuse. For these features, Modelica is widely used in industry and research for modelling and simulation of cyber physical systems.

Dymola Environment

Several environments for the Modelica language exist. For current analysis, the Dymola (version 2019, Dassault Systemes, Paris, France) has been chosen for its compatibility with the ClaRa library.

ClaRa library

To simplify the modelling process and to avoid development of components from scratch, a number of free as well as commercial Modelica libraries are available. For this study the ClaRa library was used [14] (Clasius-Rankine cycles), designed for modelling transient thermal behaviour of power plants and power systems. The ClaRa was primarily developed for the water-steam cycle and the gas path of coal dust fired boilers and heat recovery steam generators. However, with the implemented physical property models of nearly each substances used in industry today derived from the NIST database, the utilization is large. ClaRa features many benefits for the user. One of them is that it is easy enhance the code, hence creating your own models according to your requirement which perfectly meets your needs.

Several modifications had to be made to enable to model sCO2 loop CVR with ClaRa. Hence, the original source code has been extended, particularly for the shell part of the model of shell and tube heat exchanger (STHX), a model of heating rod elements and PID controllers. The extension of the model of shell part was based on the existing tube pipe model. Geometry as well as corresponding replaceable models of heat transfer and pressure drops were created to allow compatibility with the new shell model. As for the model of heating rod elements, it was based on existing wall structure and a heating source term was incorporated into the heating equation. The models of PID controllers were enhanced to enable changes of PID settings during calculations.

TUNING OF PID CONTROLLERS INTRODUCTION

For purpose of control and monitoring the sCO2 loop CVR, there is applied I&C with two independent operation workstations. The I&C manage measurements, signalization, control and adjusting of parameters and protect the technology through implemented series of safe functions in case of abnormal conditions. Further, it keeps all data archived. The I&C is built on integrated control system environment ABB

DOI: 10.17185/duepublico/48916

FREELANCE with ABB – AC900F control units and S800 I/O [21] modules directly attached on terminal units (for binary signals) and Siemens ET200M (for analog signals) [22].

Accurate control is critical to every process. As a means of ensuring that tasks such as production, distribution and treatment processes are carried out under the right conditions for the right amount of time and in the right quantities, control devices form a crucial part of virtually every industrial process. Currently the PID algorithm is the most popular feedback controller used in industry. Having a three term functionality that deals with transient and steady-state responses, the PID controller offers a simple, inexpensive, yet robust algorithm that can provide excellent performance, despite the varied dynamic characteristics of the process or plant being controlled [23]. To get the best out of the PID controllers, many tuning techniques have been developed over the past several decades. The very first techniques are dated to 1942 when Ziegler and Nichols published their paper. They have come with a closed-loop and open-loop method. The principles of these methods still provide the foundation of many of the auto tune algorithms used in many modern industrial applications. Despite its simplicity, the Ziegler Nichols closed loop method can take a long time to perform and also has the potential to create uncontrolled oscillations, which affects control stability. Eleven years after Ziegler and Nichols published their findings, in 1953, Cohen and Coon published a new tuning method. Like the Ziegler-Nichols open loop rules, the Cohen-Coon rules aim for a quarter-amplitude damping response. The Cohen-Coon tuning rules are suited to a wider variety of processes than the Ziegler-Nichols tuning rules. The Ziegler-Nichols rules work well only on processes where the dead time is less than half the length of the time constant. The Cohen-Coon tuning rules work well on processes where the dead time is less than two times the length of the time constant (and it can be stretched even further if required) [16]. Hence, the Cohen-Coon method has been used in this paper.

It is often forgotten or simply not known that different tuning rules were developed for different versions of the PID controller algorithm. The engineer responsible for tuning a control loop must be aware of the form of the algorithm used for the PID controller. The main PID structures (Interactive, Non-interactive and parallel) are very well described in [16]. The Cohen-Coon rule, used in this paper, utilizes the Non-interactive algorithm. The algorithm is described in equation (1).

$$\boldsymbol{CO} = \boldsymbol{K_c} \cdot \left(\boldsymbol{e(t)} + \frac{\mathbf{1}}{\boldsymbol{T_i}} \int \boldsymbol{e(t)}\, \boldsymbol{dt} + \boldsymbol{T_d} \frac{\boldsymbol{de(t)}}{\boldsymbol{dt}} \right) \quad (1)$$

The Cohen-Coon tuning rule uses three process characteristics: process gain (GP), dead time (td), and time constant (Tau). These are determined by doing a step test and analyzing the results. In order to derive these characteristics, the PID controller which is subject of the tuning needs to be in manual and the system has to be stabilized. A step change in the controller output (CO) is introduced and after the process variable (PV) stabilizes at a new value, the characteristics can be determined according to Figure 9. The size of this step should be large enough that the process variable moves well clear of the process noise/disturbance level.

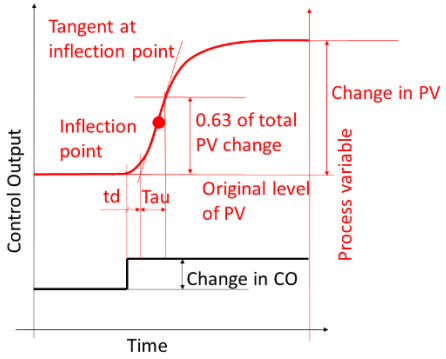

Figure 9: Schematic figure of Cohen-Coon characteristics.

Calculation of new tuning settings using the Cohen-Coon tuning rule is described in Table 6.

Table 6: Cohen-Coon rule [16].

	K_c	T_i	T_d
P controller	$\frac{1.03}{GP}\left(\frac{Tau}{td}+0.34\right)$		
PI controller	$\frac{0.9}{GP}\left(\frac{Tau}{td}+0.092\right)$	$3.33td\left(\frac{Tau+0.092td}{Tau+2.22td}\right)$	
PD controller	$\frac{1.24}{GP}\left(\frac{Tau}{td}+0.129\right)$		$0.27td\left(\frac{Tau-0.324td}{Tau+0.129td}\right)$
PID controller	$\frac{1.35}{GP}\left(\frac{Tau}{td}+0.185\right)$	$2.5td\left(\frac{Tau+0.185td}{Tau+0.611td}\right)$	$0.37td\left(\frac{Tau}{Tau+0.185td}\right)$

One has to be careful when calculating the process gain GP according to equation (2), since normalized values needs to be implemented, i.e. the total change obtained in PV has to be converted to a percentage of the span of the measuring device. Similarly to the change of CO in percentage.

$$\boldsymbol{GP} = \frac{\boldsymbol{change\ in\ PV}\ [\%]}{\boldsymbol{change\ in\ CO}\ [\%]} \quad (2)$$

TUNING OF PID CONTROLLERS AND COMPARISON WITH MEASSURED DATA

There are number of different control loops in the sCO2 loop at CVR. However, as the control mode is most often associated with temperature, hence the temperature controller at the outlet of the heater 2 (H2) was selected to be subject of this work.

As described in previous chapter, the Cohen-Coon method is used in this paper to determined PID controller constant. Two step changes in the heater 2 (H2) during a stabilized system were introduced and process variable (T_CO2_H2_out - 1LKD40CT004) curves have been generated.

Step-up

Firstly, a sudden step-up increase in H2 power output (from initial 6.2 kW to final 10.9 kW) was initiated at stable system. The response curve of the process variable (temperature outlet from H2) is shown in Figure 10.

DOI: 10.17185/duepublico/48916

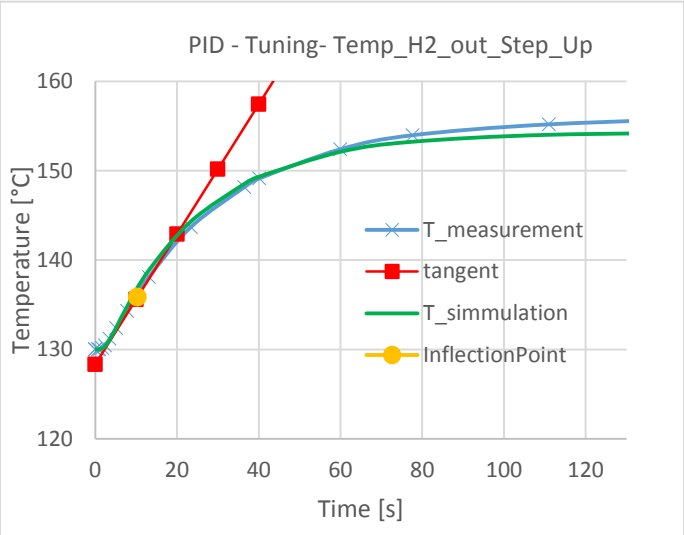

Figure 10: Response curve of temperature outlet from H2 during step-up test.

Step-down

In order to verify the first test, second step test was conducted after the stabilization of parameters in the system. A sudden step-down decrease in H2 power output (from initial 10.9 kW to final 6.6 kW) was initiated at stable system. The response curve of the process variable (temperature outlet from H2) is shown in Figure 11.

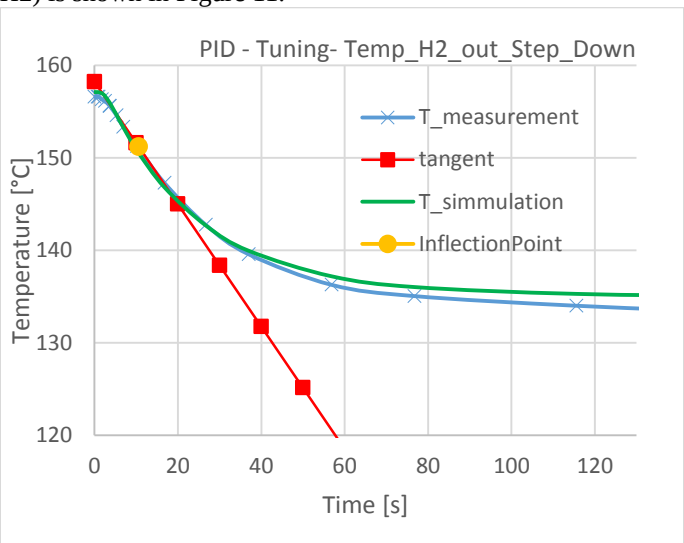

Figure 11: Response curve of temperature outlet from H2 during step-down.

In both cases, the simulated results from the ClaRa model follows the measured values of the process variable very well. The total maximum error calculated from absolute temperatures in Kelvins, does not exceeds 0.5 %.

Table 7 summarizes the PID tuning settings from both tests including the settings derived from simulations. Note that calculated controller gain (Kc) is according to recommendation [16] divided the by two to reduce overshoot and improve stability. For clarity, the process gain (GP) was calculated as follows (the step-up experimental values are shown):

$$GP = \frac{\frac{change\ in\ PV\ [K]}{range\ of\ PV\ [K]}}{\frac{change\ in\ CO\ [kW]}{range\ of\ CO\ [kW]}} = \frac{\frac{155.3-130}{600-0}}{\frac{10.9-6.2}{30-0}} = \mathbf{0.27} \quad (3)$$

Table 7: PID tuning settings for measured and simulated data

	Kc	Ti	Td
Step-up test – measured	29.14	5.60	0.85
Step-down test - measured	26.79	5.97	0.90
Average - measured	27.96	5.79	0.88
Step-up test – simulated	26.79	5.35	0.81
Step-down test - simulated	26.33	5.24	0.79
Average - simulated	26.56	5.30	0.80

The PID constants obtained from both experimental tests are in very good agreement. The discrepancy of the PID sets derived from simulations and experiment is within 10%. One of the possible explanation for error results from the fact that the dead time for both test cases are relatively small (around 2.2 s), hence even a small error (of few tenths of seconds) in determination the dead time from the tangent line at inflection point can lead to significant inaccuracy in the PID constants.

In order to provide complete data for benchmark exercises, all relevant parameters of the sCO2 loop CVR at steady state conditions, prior to the step changes, are summarized in ANNEX G. In addition, the simulated results are shown, providing further evidence about the capability of the numerical code capturing the measured values.

TUNING OF PID CONTROLLERS FOR MULTIPLE PROCESS CONDITIONS

Fluid properties of the sCO2 near the critical point experiences highly non-linear variations. This is one of the key enabling features for the sCO2, however on the other hand, it presents challenges for modeling, and exhibits unique behavior during transients which greatly complicate the control of the system. To demonstrate that series of response curves with different conditions (pressure 10 MPa ÷ 20 MPa, temperature 30 °C ÷ 400 °C) were simulated and tuning constants of the PID controller were derived using Cohen-Coon method for each case. Once again, the temperature outlet from heater H2 was selected as a process variable. Notice that the parametric values of pressures stated here are meant to be pressures at the heater H2 where the response test took place, i.e. high pressure side of the loop (from outlet of the main circulation pump to reduction valve). Further, mass flow rate through the sCO2 loop was kept constant at 0.13 kg/s and so do the low pressure values (7.65 MPa) to maintain a core of similarity with the PID tuning in the previous chapter. Hence, 10 MPa at the high pressure side was the minimum value for a given low pressure 7.65 MPa taking into account the pressure losses through the loop.

The resulted tuned controller gains (Kc) for different conditions in the sCO2 loop are plotted in Figure 12. Since the

DOI: 10.17185/duepublico/48916

integral and derivative time constants did not varied significantly and stayed in a relatively small range (Ti = 4 s ÷ 6 s and Td = 0.6 s ÷ 1 s), they are not shown here explicitly. From the Figure 12 it can be observed that the controller gains follow the behavior of heat capacity. The specific heat capacity (cp) is peaking at so called pseudo-critical temperatures and similarly the controller gains. This effect is growing closer it gets to the critical pressure. The behavior of controller gains can be explained as follows. Where the cp is higher, there the PID controller needs higher gain in order to have sufficiently fast response. On the other hand, where cp is smaller, there the PID controller needs lower gain not to cause oscillations. Note that controller gains are gain divided the by two to reduce overshoot and improve stability.

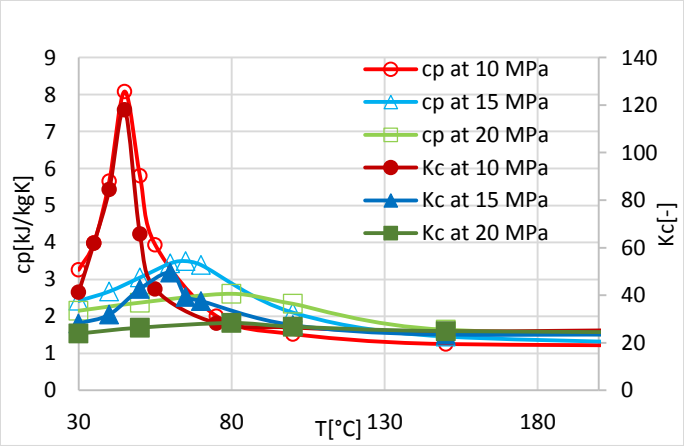

Figure 12: Calculated values of controller gains and specific heat capacities at different pressures and temperatures.

Once the new sets of PID controller were derived, they were tested on several examples. Following figures Figure 13, Figure 14 and Figure 15 shows the behavior of PID controller of the temperature outlet from H2 during the step change of set point. For demonstration, two extreme PID sets were chosen together with manually tuned constants. One extreme case represents the parameters tuned for the highest cp approx. 8 $kJ \cdot kg^{-1} \cdot K^{-1}$ (Kc=118, Ti=3.7 s, Td=0.6 s) and the other for the lowest cp approx. 1 $kJ \cdot kg^{-1} \cdot K^{-1}$ (Kc=25, Ti=5 s, Td=1 s). Both were derived from previous calculation tuned by Cohen-Coon method. For the manually tuned PID following constants were used (Kc=25, Ti=20 s, Td=1 s), i.e. the setting was the same as for the case with the lowest cp, only the integral time constant quadrupled.

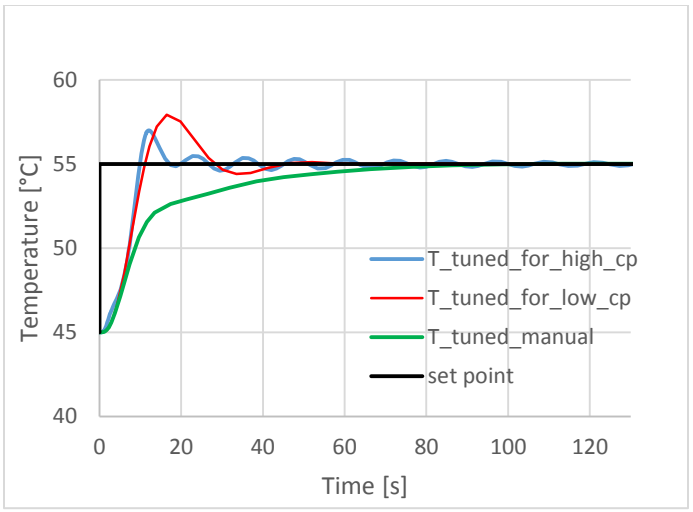

Figure 13: Outlet temperatures of H2 at 10MPa controlled by PID with different settings (set point at 45°C).

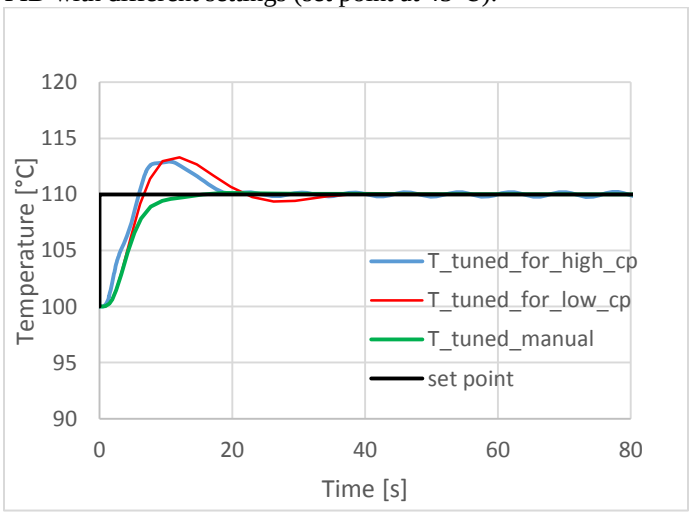

Figure 14: Outlet temperatures of H2 at 10MPa controlled by PID with different settings (set point at 100°C).

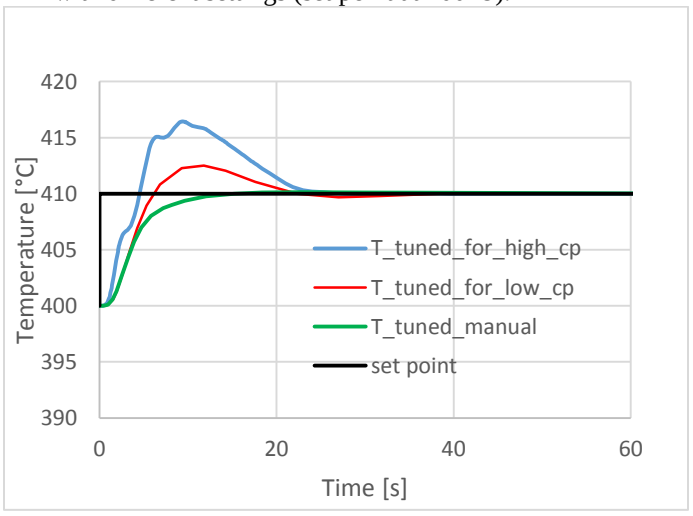

Figure 15: Outlet temperatures of H2 at 10MPa controlled by PID with different settings (set point at 400°C).

DOI: 10.17185/duepublico/48916

It can be observed that the process variable, controlled by PID with settings tuned for high cp, exhibits comparatively high overshoots and instabilities, especially for the higher temperatures test cases (above 100°C). Improvement can be seen for the low cp tuning. It still exhibits quite high overshoots, however the oscillations were significantly reduced. The manually tuned controller behaves well for all 3 tested temperatures. It shows no overshoots, no oscillations, only for the test at 45°C, time for the process variable to settle is quite long (100 s) and it could be improve by increasing the controller gain.

CONCLUSION

The paper shows a comprehensive insight into the experimental investigations and simulations of the sCO2 loop in CVR. Rather than focusing on separate component behavior, this study aims on a system level (component interaction) for both steady states and dynamic transients including control system interactions and PID tuning techniques. Particularly, this paper contains valuable experimental data of the sCO2 loop and their comparison with simulations.

The first part of the paper presents the sCO2 loop, and shows its configuration and specifications. This includes the design parameters of all main components as well as the P&I diagram with measurements and their positions in the system and the piping. Altogether three sets of measured steady states data are outlined and together with detail description of the loop it gives necessary information for performing the benchmark exercise on numerical codes. Such a benchmark was performed with the open source Modelica-based code ClaRa using the simulation environment DYMOLA 2019. The simulated results show fair agreement with measured data, demonstrating reasonable accuracy of the simulation tool. There are maximum 2.5 K/0.2 MPa/0.6 kW temperature/pressure/heating power errors respectively. Further measurements and simulations were carried out, particularly transients, however it is out of the page limit for the paper. Hence, the results of these analyses will be published somewhere else.

Once the numerical model on steady states was validated, the transient tests covering the tuning procedure of the PID controllers were performed. The scope of the study is to give a first approximation of tuning parameters of such a system. For this purpose, one of the most utilized tuning technique, the Cohen-Coon (C-C) method, was deployed. The temperature controller at the outlet of the heater 2 (H2) was selected to be subject of this work. A sudden step-up/step-down increase/decrease in H2 power output respectively at a given condition was executed. The response temperature curves were analyzed and PID constants for the controller were calculated. The PID constants obtained from both experimental tests are in very good agreement. The discrepancy of the PID sets derived from simulations and experiment is within 10%.

For the sake of highly non-linear behavior of sCO2, series of response curves with different conditions (pressure 10 MPa ÷ 20 MPa, temperature 30 °C ÷ 400 °C) were simulated in order to find the optimum PID settings for all prospective conditions for sCO2 loop in CVR. It was observed that the resulted controller gains follow behavior of the specific heat capacity, hence they were peaking at the pseudocritical points. This naturally intensifies closer it gets to the supercritical pressure. Hence, near the pseudocritical temperatures and supercritical pressures the PID would need to be given various customized sets of constants for particular conditions. Far from the pseudocritical temperatures, single PID setting should be sufficient.

Once the new sets of PID controller were derived, they were tested on several examples. It has been found that the tuned PID constants according to C-C method exhibits relatively high overshoots. It is due to the fact that different tuning techniques gives preferences to fast response prior to stable behavior. The results from the paper indicates that C-C method prefers fast response. Hence, if one would like to use sole set of PID for all different conditions then it is recommended to use the settings tuned for lower values of cp, i.e. with lower controller gain. Otherwise, the system might oscillates in low cp regions. One has to understand that derived PID constants according to C-C method are just first approximations and further manual tuning are inevitable. In this paper the manually tuned parameters were based on the C-C tuning setting for low cp case and only the integral time constant was quadrupled. With this PID setting the performance of the controller was very much improved with practically representative actions.

Further investigations are planed including deployment of several other tuning techniques in order to improve predictions of the PID settings. In addition, other control loops of the sCO2 experimental facility in CVR, i.e. mass flow through the cycle driven by circulation pump with frequency convertor or pressure in the system driven by reduction valve etc., are prospective to be tested.

NOMENCLATURE

cp	Specific heat capacity, $J \cdot kg^{-1} \cdot K^{-1}$
D	Diameter, m
e(t)	Error (Set point – Process variable)
H	Enthalpy, $J \cdot kg^{-1}$
K_c	Controller gain
Kv	Flow coefficient of the valve, $m^3 \cdot h^{-1}$
Kvs	Kv at a fully-open valve position, $m^3 \cdot h^{-1}$
L	Length, m
$\dot{m}$	Mass flow, $kg \cdot s^{-1}$
p	Pressure, Pa
P	Power, W
T	Temperature, K
T_i	Integral time constant
T_d	Derivative time constant
ρ	Density, $kg \cdot m^{-3}$

DOI: 10.17185/duepublico/48916

ACRONYMS

C-C	Cohen-Coon
CH1	Water cooler
CH2	Oil cooler
CO	Control output signal of PID controller
GP	Process gain
H1/1	Electric heater
H1/2	Electric heaters
H2	Electric heaters
H3	Electric heaters
HP	High pressure
HTR	High temperature regenerative heat exchanger
I&C	Instrumentation and control system
KKS	Identification system for power plants
LP	Low pressure
LTR	Low temperature regenerative heat exchanger
MP	Main pump
PID	Proportional Integral Derivative
P&ID	Piping and instrumentation diagram
PV	Process value
RV	Reduction valve
sCO2	Supercritical CO_2
td	Dead time (time difference between the change in CO and the intersection of the tangential line and the original PV level)
Tau	Time constant (time difference between intersection at the end of dead time, and the PV reaching 63% of its total change)
STHX	Shell and tube heat exchanger

ACKNOWLEDGEMENTS

This paper has been conducted within the sCO2-Flex project which has received funding from the European Union's Horizon 2020 research and innovation programme under grant agreement N° 764690.

REFERENCES

[1] DOSTAL V.: A supercritical carbon dioxide cycle for next generation nuclear reactors [Ph.D. thesis]. Department of Nuclear Engineering, Massachusetts Institute of Technology (MIT); 2004.

[2] BRUN K.; FRIEDMAN P.; DENNIS R.: Fundamentals and Applications of Supercritical Carbon Dioxide (SCO2) Based Power Cycles. 1st edition, Elsevier Science & Technology, 2017.

[3] MENDEZ, C.M., ROCHAU G.: sCO2 Brayton Cycle: Roadmap to sCO2 Power Cycles NE Commercial Applications, SANDIA REPORT, SAND2018-6187, Printed June 2018, Albuquerque, New Mexico.

[4] CAGNAC, A., 2018, "The supercritical co2 cycle for flexible & sustainable support to the electricity system (sco2-flex)," Electricité de France, Avenue de Wagram 22, 75008, Paris 08, Accessed Apr. 4, 2019, http://www.sco2-flex.eu/.

[5] BRINGER, R.P.; SMITH, J.M.: Heat transfer in the critical region. AIChE J. 3 (1), 49–55, 1957.

[6] PETUKHOV, B.S.; KRASNOSCHEKOV, E.A.; PROTOPOPOV, V.S.: An investigation of heat transfer to fluids flowing in pipes under supercritical conditions. In: International Developments in Heat Transfer: Papers presented at the 1961 International Heat Transfer Conference, ASME, University of Colorado, Boulder, Colorado, USA, 8–12 January, Part III, Paper 67, pp. 569–578, 1961.

[7] DUFFEY, R.B.; PIORO, I.L.: Experimental heat transfer of supercritical carbon dioxide flowing inside channels (survey), Nuclear Engineering and Design 235 (2005) 913–924.

[8] VOJACEK, A. ET AL.: Challenges in supercritical CO2 power cycle technology and first operational experience at CVR, 2nd European sCO2 Conference, Duisburg-Essen, August 2018, DOI: 10.17185/duepublico/46075.

[9] WRIGHT, S.A. ET AL.: Operation and Analysis of a Supercritical CO2 Brayton Cycle, SAND2010-0171, Albuquerque, New Mexico, Sep. 2010.

[10] UTAMURA, M. ET. AL.: Demonstration of supercritical CO2 closed regenerative brayton cycle in a bench scale experiment. Proceedings of ASME Turbo Expo 2012, June 11-15, 2012, Copenhagen, Denmark, GT2012-68697.

[11] HACKS A. J.; VOJACEK A.; DOHMEN H. J.; BRILLERT D.: Experimental Investigation of the sCO2-HeRo Compressor. 2018-sCO2.eu-115, 2nd European supercritical CO2 Conference, August, 2018.

[12] AHN, Y. ET. AL.: Design consideration of supercritical CO2 power cycle integral experiment loop, Energy 86 (2015) 115-127.

[13] CHO, J. ET. AL.: Research on the development of a small-scale supercritical carbon dioxide power cycle experimental test loop, The 5th International Symposium - Supercritical CO2 Power Cycles, March 28-31, 2016, San Antonio, Texas.

[14] NIELSEN, L.: TLK-Thermo GmbH, "Dyncap/Dynstart | ClaRa – Simulation of Clausius-Rankine cycles | TLK-Thermo GmbH, Braunschweig | XRG Simulation GmbH, Hamburg | Institut für Thermofluiddynamik (TUHH), Hamburg | Institut für Energietechnik (TUHH), Hamburg." [Online]. Available: https://www.claralib.com/. [Accessed: 4-Apr-2019].

[15] COHEN, G. H.; G. A. COON (1953): "Theoretical consideration of retarded control."Trans. ASME, 75, pp. 827-834.

[16] SMUTS, J.F.: Control notes – Reflection of a process control practitioner. [Online]. Available: http://blog.opticontrols.com. [Accessed: 4-Apr-2019].

[17] Division Isover, Saint-Gobain Construction Products CZ a.s., Masarykova 197, 517 50 Častolovice. [Online].

DOI: 10.17185/duepublico/48916

Available: https://www.isover.cz/en/products/orstech-dp-100. . [Accessed: 4-Apr-2019].
[18] CASELLA F.; LEVA, A.: “Modelling of thermo-hydraulic power generation processes using Modelica,” Math. Comput. Model. Dyn. Syst., vol. 12, no. 1, pp. 19–33, Feb. 2006.
[19] KOFRANEK, J. ET. AL.: “Causal or acausal modeling: labour for humans or labour for machines,” in Technical Computing Prague, 2008, pp. 1–16.
[20] NIST Reference Fluid Thermodynamic and Transport Properties Database (REFPROP): Version 10.
[21] Ulrich Spiesshofer, ABB Asea Brown Boveri Ltd, Affolternstrasse 44, 8050 Zurich, Switzerland Available: https://new.abb.com/control-systems/essential-automation/freelance. [Accessed: 4-Apr-2019].
[22] Siemens Aktiengesellschaft Werner-von-Siemens-Straße 1, 80333 Munich, Germany Available: https://w3.siemens.com/mcms/distributed-io/en/ip20-systems/et200m/interface-modules/pages/default.aspx. [Accessed: 4-Apr-2019].
[23] LI, Y.; ANG, K.H.; CHONG, G.C.Y. (2006) PID control system analysis and design. IEEE Control Systems Magazine 26(1):pp. 32-41.
[24] ZIEGLER, J. G.; NICHOLS, N.B.: “Optimum Settings for Automatic Controllers,” Transactions of the ASME, Vol. 64, 1942, pp. 759-768.

DOI: 10.17185/duepublico/48916

ANNEX A

PIPING AND INSTRUMENTATION DIAGRAM (P&ID) OF THE SCO2 LOOP, CVR

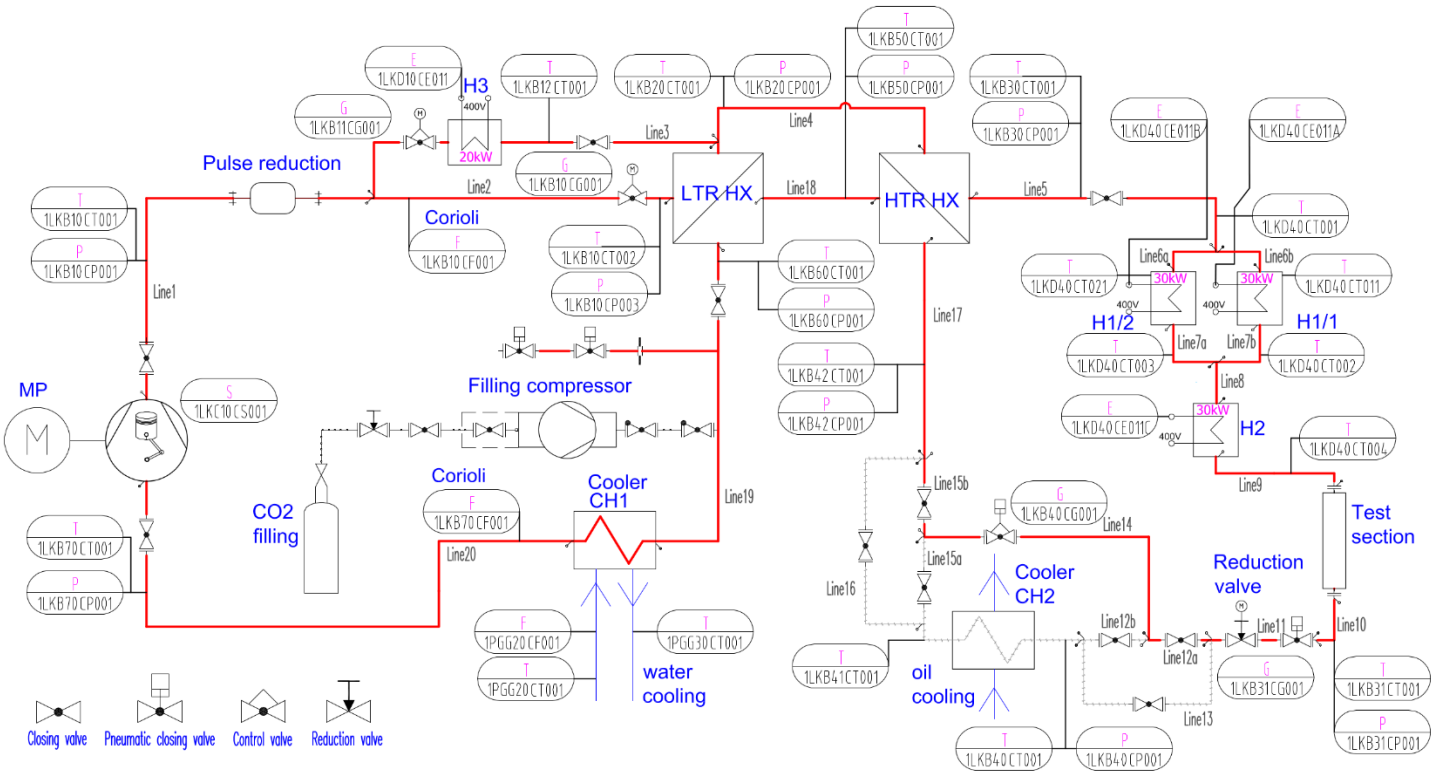

ANNEX B

UNCERTAINTY OF THE MEASUREMENT DEVICES IN SCO2 LOOP, CVR

Variable	Range	Unit	Description	Device error	Transducer error	Input card error	Control system error	Total error
$\dot{m}_{sCO2}$	0 - 0.7	kg/s	mass flow rate 1LKB10CF001, 1LKB70CF00 1Rheonik (RHM12)	0.15 % from 1.66 kg/s	Rawet - PX310S	Siemens SM 331	ABB freelance	+/- 0.007 kg/s
					0.1 % from range	0.4 % from range	0.1 % from range	
T_{sCO2}	0 - 600	°C	TC (type K) T_{sCO2}, Omega	+/- 0.5 K for (0÷100°C) +/- 0.6 K for 300°C +/- 1.4 K for 500°C	Rawet - PX310S	Siemens SM 331	ABB freelance	+/- 4.1 K for (0÷100°C) +/- 4.2 K for 300°C +/- 5 K for 500°C
					0.1 % from range	0.4 % from range	0.1 % from range	
p_{sCO2_LP}	0 - 15	MPa	sCO2 pressures at low pressure side of	0.15 % from range	Rawet - PX310S	Siemens SM 331	ABB freelance	+/- 0.11 MPa

DOI: 10.17185/duepublico/48916

			the loop, GE (UNIK 5000)		0.1 % from range	0.4 % from range	0.1 % from range	
$p_{\_sCO2\_HP}$	0 - 30	MPa	sCO_2 pressures at high pressure side of the loop , GE (UNIK 5000)	0.15 % from range	Rawet - PX310S	Siemens SM 331	ABB freelance	+/- 0.23 MPa
					0.1 % from range	0.4 % from range	0.1 % from range	
$P_{\_H1/1-2}$ $P_{\_H2,3}$	0 - 30	kW	electric power of heaters, MT Brno	0.75 % from range	Rawet - PX310S	Siemens SM 331	ABB freelance	+/- 0.4 kW
					0.1 % from range	0.4 % from range	0.1 % from range	
$T_{\_water}$	0 - 120	°C	water temperature of the cooling circuit, JSP (Pt 100)	0.15K+0.2 % from range	Rawet - PX310S	Siemens SM 331	ABB freelance	+/- 1.1 K
					0.1 % from range	0.4 % from range	0.1 % from range	
$\dot{m}_{water}$	0 – 3.8	kg/s	water mass flow rate of the cooling circuit, turbine flowmeter, Hoffer	1.1 % from range	-	-	ABB freelance	+/- 0.046 kg/s
					-	-	0.1 % from range	

ANNEX C

UNCERTAINTY OF THE MEASUREMENT DEVICES IN SCO2 LOOP, CVR

Component	Geometry
HTR + LTR (counter-flow shell and tube-type from SS 321)	Length of HTR = 20 m (2 x U-tube vertical), 3 x 2 = 6 high pressure flanges Ø 110 mm (height 25 mm) and the same 6 low pressure flanges Length of LTR = 60 m (6 x U-tube vertical), 7 x 2 = 14 high pressure flanges Ø 110 mm (height 25 mm) and the same 14 low pressure flanges Number of internal tubes = 7, Internal tube Ø 10 x 1.5 mm, Shell Ø 50 x 5 mm.
H1/1 + H1/2 (30 + 30 kW) (from SS 321)	Length = 0.95 m, Number of heating rods = 2 x 6, Diameter of a heating rod Ø 8 mm (cladding tube Ø 8 x 1 mm SS 321, ceramic (MgO) filling Ø 6 x 1 mm, ceramic (Al2O3) filling Ø 4 x 1.75 mm, Ø 0.5 mm wire Kanthal alloy (FeCrAl)), Shell Ø 100 x 20 mm, guiding tube Ø 36 x 2 mm with plugs on both ends
H2 (30 kW) (from Inconel 625)	Length = 0.95 m, Number of heating rods = 2 x 6, Diameter of a heating rod 8 mm (ceramic filling and wire as in H1/1 + H1/2), Shell Ø 73 x 6.5 mm, 2 x 1 = 2 flanges Ø 110 mm (height 25 mm), guiding tube Ø 36 x 2 mm with plugs on both ends
H3 (20 kW) (from SS 321)	Length = 0.75 m, Number of heating rods = 2 x 6, Diameter of a heating rod Ø 8 mm (ceramic filling and wire as in H1/1 + H1/2), Shell Ø 100 x 20 mm, guiding tube Ø 36 x 2 mm with plugs on both ends
CH1 (counter-flow shell and tube-type from SS)	Length = 7.5 m, Number of internal tubes = 7, Internal tube Ø 10 x 1.5 mm, Shell Ø 43 x 1.5 mm
CH2 (counter-flow shell and tube-type from Inconel 625 (CO2 side)/SS 321 (oil side))	Length = 1.8 m, Number of internal tubes = 7, Internal tube Ø 10 x 1.5 mm, Shell Ø 43 x 1.5 mm, 2 x 2 = 4 high flanges Ø 110 mm (height 25 mm)
TS (from Inconel 625)	Length = 2 m, Shell Ø 73 x 6.5 mm, 2 x 2 = 4 high flanges Ø 140 mm (height 26 mm)
Reduction valve (from SS 321)	Body weight 125 kg, Length = 0.5 m
Control valves (3x) (from SS 321)	Body weight 5 kg, Length = 0.3 m (each)
Closing valves	Body weight 1 kg, Length = 0.3 m

DOI: 10.17185/duepublico/48916

*("hot" part of the loop) (from SS 321)	(each)
Closing valves **("cold" part of the loop) (from SS 321)	Body weight 5 kg, Length = 0.3 m (each)

** The "hot" part of the loop is from inlet of heater H3 and inlet of high pressure LTR to outlet of low pressure LTR.*

*** The "cold" part is the rest of the loop (from outlet of low pressure LTR to inlet to heater H3 and inlet of high pressure LTR.*

ANNEX D

PIPELINE GEOMETRY OF THE SCO_2 LOOP

Line 1	Pipeline from MP to T-junction LTR by-pass	Length = 2.6 m, 1x90° Bend, Tube Ø 22 x 4 mm
Line 2	Pipeline from T-junction LTR by-pass to LTR	Length = 6.8 m, 6x90° Bend, Tube Ø 22 x 4 mm
Line 3	LTR by-pass	Length = 7.6 m, 2x90° Bend, Tube Ø 22 x 4 mm
Line 4	Pipeline from outlet of high pressure LTR to inlet of high pressure HTR	Length = 0.7 m, 2x90° Bend, Tube Ø 22 x 4 mm
Line 5	Pipeline from outlet of high pressure HTR to T-junction at the inlet of H1/1 and H1/2	Length = 1 m, 1x90° Bend, Tube Ø 22 x 4 mm
Line 6a/6b	2 identical pipelines from T-junction at the inlet of H1/1 and H1/2 to H1/1 and H1/2	Length = 1.4 m, 1x60° Bend, Tube Ø 22 x 4 mm
Line 7a/7b	2 identical pipelines from H1/1 and H1/2 to T-junction at the outlet of H1/1 and H1/2	Length = 1.5 m, 1x60° Bend, Tube Ø 22 x 4 mm
Line 8	Pipeline from T-junction outlet of H1/1 and H1/2 to H2	Length = 1.9 m, 2x90° Bend, Tube Ø 22 x 4 mm
Line 9	Pipeline from H2 to test section	Length = 2 m, 2x90° Bend, Tube Ø 22 x 4 mm
Line 10	Pipeline from test section to reduction valve	Length = 1.9 m, 1x90° Bend, Tube Ø 22 x 4 mm
Line 11	Pipeline from reduction valve to T-junction of line 12a/13	Length = 8.4 m, 8x90° Bend, Tube Ø 20 x 3 mm
Line 12a	Pipeline from T-junction of line 12a/13 to T-junction CH2 by-pass (inlet of CH2 by-pass)	Length = 0.4 m, 1x60° Bend, Tube Ø 20 x 3 mm
Line 12b	Pipeline from T-junction CH2 by-pass (inlet of CH2 by-pass) to T-junction of line 12b/13	Length = 0.4 m, 1x60° Bend, Tube Ø 20 x 3 mm
Line 13	Pipeline from T-junction of line 12a/13 to T-junction of line 12b/13 to	Length = 0.9 m, 2x60° Bend, Tube Ø 20 x 3 mm
Line 14	Pipeline CH2 by-pass	Length = 5.5 m, 4x90° Bend, Tube Ø 20 x 3 mm
Line 15a	Pipeline from T-junction of line 15a/16 to T-junction CH2 by-pass (outlet of CH2 by-pass)	Length = 0.4 m, 1x60° Bend, Tube Ø 20 x 3 mm
Line 15b	Pipeline from T-junction CH2 by-pass (outlet of CH2 by-pass) to T-junction of line 15b/16	Length = 0.4 m, 1x60° Bend, Tube Ø 20 x 3 mm
Line 16	Pipeline from T-junction of line 15a/16 to T-junction of line 15b/16	Length = 0.9 m, 2x60° Bend, Tube Ø 20 x 3 mm
Line 17	Pipeline from T-junction of line 15b/16 to inlet of low pressure HTR	Length = 0.8 m, 1x90° Bend, Tube Ø 20 x 3 mm
Line 18	Pipeline from outlet of low pressure HTR to inlet of low pressure LTR	Length = 0.7 m, 2x90° Bend, Tube Ø 22 x 4 mm
Line 19	Pipeline from outlet of low pressure LTR to CH1	Length = 1.8 m, 2x90° Bend, Tube Ø 20 x 3 mm
Line 20	Pipeline from CH1 to MP	Length = 4.4 m, 7x90° Bend, Tube Ø 20 x 3 mm

ANNEX E
POSITION OF THE MEASUREMENT SENSORS

Measurement type	**Position**	**Pipeline**
m_CO2_MP (1LKB70CF001)	3.9 m prior to MP inlet	line 20
m_CO2_LTR (1LKB10CF001)	1.6 m from MP outlet	line 1
rotational speed_MP (1LKC10CS001)	MP	line 1
power_H1/1 (1LKD40CE011A)	H1/1	line 6b,7b
power_H1/2 (1LKD40CE011B)	H1/2	line 6a,7a
power_H2 (1LKD40CE011C)	H2	line 8,9
power_H3 (1LKD10CE011)	H3	line 3
p_CO2_MP_in (1LKB70CP001)	3.4 m prior to MP inlet	line 20
T_CO2_MP_in (1LKB70CT001)	5.1 m prior to MP inlet	line 20
p_CO2_MP_out (1LKB10CP001)	1.6 m from MP outlet	line 1
T_CO2_MP_out (1LKB10CT001)	1.6 m from MP outlet	line 1
position_valve_LTR_in (1LKB10CG001)	control valve LTR inlet	line 2
position_valve_LTR_by-pass (1LKB11CG001)	control valve LTR by-pass	line 3
T_by-pass LTR (1LKB12CT001)	0.8 m from H3 outlet	line 3
p_CO2_LTR_p_high_side_in (1LKB10CP003)	LTR high pressure inlet	line 2
T_CO2_LTR_p_high_side_in (1LKB10CT002)	LTR high pressure inlet	line 2
p_CO2_LTR_p_high_side_out (1LKB20CP001)	HTR high pressure inlet	line 4
T_CO2_LTR_p_high_side_out (1LKB20CT001)	HTR high pressure inlet	line 4
T_CO2_HTR_p_high_side_out (1LKB30CT001)	HTR high pressure outlet	line 5
p_CO2_HTR_p_high_side_out (1LKB30CP001)	HTR high pressure outlet	line 5
T_CO2_H1/1_H1/2_in (1LKD40CT001)	H1/1, H1/2 inlet (T-junction)	line 5
T_CO2_H1/1_out (1LKD40CT002)	H1/1, H1/2 outlet (T-junction)	line 7b
T_CO2_H1/2_out (1LKD40CT003)	H1/1, H1/2 outlet (T-junction)	line 7a
T_CO2_H2_out (1LKD40CT004)	1.2 m from H2 outlet	line 9
p_CO2_RV_in (1LKB31CP001)	TS outlet	line 10

DOI: 10.17185/duepublico/48916

T_CO2_RV_in (1LKB31CT001)	TS outlet	line 10
position of RV (1LKB31CG001)	RV	line 11
position_valve_CH2_by-pass (1LKB40CG001)	control valve CH2 by-pass	line 14
p_CO2_HTR_p_low_side_in (1LKB42CP001)	HTR low pressure inlet	line 17
T_CO2_HTR_p_low_side_in (1LKB42CT001)	HTR low pressure inlet	line 17
p_CO2_HTR_p_low_side_out (1LKB50CP001)	HTR low pressure outlet	line 18
T_CO2_HTR_p_low_side_out (1LKB50CT001)	HTR low pressure outlet	line 18
p_CO2_LTR_p_low_side_out (1LKB60CP001)	LTR low pressure outlet	line 19
T_CO2_LTR_p_low_side_out (1LKB60CT001)	LTR low pressure outlet	line 19
m_H2O_CH1 (1PGG20CF001)	1.4 m prior to CH1 inlet	water circuit
T_H2O_CH1_in (1PGG20CT001)	CH1 inlet	water circuit
T_H2O_CH1_out (1PGG30CT001)	CH1 outlet	water circuit

ANNEX F
MEASSURED AND CALCULATED STEADY STATE PARAMETERS

parameter	Unit	5_meass	5_sim	error_abs	37_meass	37_sim	error_abs	61_meass	61_sim	error_abs
m_CO2_MP (1LKB70CF001)	kg/s	0.227	0.225	0.0	0.187	0.188	0.0	0.198	0.198	0.0
m_CO2_LTR (1LKB10CF001)	kg/s	0.227	0.225	0.0	0.187	0.188	0.0	0.198	0.198	0.0
power_H1/1 (1LKD40CE011A)	kW	0.806	0.959	-0.2	6.539	6.731	-0.2	3.077	2.676	0.4
power_H1/2 (1LKD40CE011B)	kW	0.932	0.959	0.0	6.688	6.731	0.0	3.190	2.676	0.5
power_H2 (1LKD40CE011C)	kW	26.865	27.452	-0.6	17.634	17.672	0.0	28.075	28.022	0.1
power_H3 (1LKD10CE011)	kW	0.000	0.000	0.0	0.000	0.000	0.0	0.000	0.000	0.0
p_CO2_MP_in (1LKB70CP001)	MPa	8.821	8.841	0.0	7.502	7.529	0.0	7.968	7.989	0.0
T_CO2_MP_in (1LKB70CT001)	°C	21.259	21.172	0.1	19.267	19.291	0.0	16.913	16.916	0.0
p_CO2_MP_out (1LKB10CP001)	MPa	19.820	19.997	-0.2	20.591	20.806	-0.2	19.920	20.177	-0.3
T_CO2_MP_out (1LKB10CT001)	°C	33.980	35.394	-1.4	38.708	36.335	2.4	30.709	31.384	-0.7
position_valve_LTR_in (1LKB10CG001)	%	100.000	100.000	0.0	100.000	100.000	0.0	100.000	100.000	0.0
position_valve_LTR_by-pass (1LKB11CG001)	%	0.000	0.000	0.0	0.000	0.000	0.0	0.000	0.000	0.0
p_CO2_LTR_p_high_side_in (1LKB10CP003)	MPa	19.828	19.944	-0.1	20.624	20.767	-0.1	19.944	20.136	-0.2
T_CO2_LTR_p_high_side_in (1LKB10CT002)	°C	32.697	35.059	-2.4	36.755	35.920	0.8	29.060	31.102	-2.0
T_CO2_HTR_p_high_side_out (1LKB30CT001)	°C	70.975	71.993	-1.0	208.699	206.823	1.9	342.986	343.688	-0.7
p_CO2_HTR_p_high_side_out (1LKB30CP001)	MPa	19.670	19.794	-0.1	20.506	20.655	-0.1	19.808	19.994	-0.2
T_CO2_H1/1_H1/2_in (1LKD40CT001)	°C	71.363	71.945	-0.6	209.193	206.702	2.5	344.299	343.570	0.7
T_CO2_H1/1_out (1LKD40CT002)	°C	75.001	75.000	0.0	259.999	260.000	0.0	365.060	365.000	0.1
T_CO2_H1/2_out (1LKD40CT003)	°C	74.996	75.000	0.0	259.989	260.000	0.0	365.055	365.000	0.1
T_CO2_H2_out (1LKD40CT004)	°C	122.019	123.820	-1.8	328.064	329.504	-1.4	470.081	472.544	-2.5
p_CO2_RV_in (1LKB31CP001)	MPa	19.697	19.700	0.0	20.508	20.510	0.0	19.768	19.770	0.0
T_CO2_RV_in (1LKB31CT001)	°C	123.183	123.471	-0.3	328.633	328.275	0.4	470.068	470.686	-0.6
position of RV (1LKB31CG001)	%	63.000	63.000	0.0	57.000	57.000	0.0	60.000	60.000	0.0
position_valve_CH2_by-pass (1LKB40CG001)	%	100.000	100.000	0.0	100.000	100.000	0.0	100.000	100.000	0.0
p_CO2_HTR_p_low_side_in (1LKB42CP001)	MPa	9.270	9.050	0.2	7.939	7.705	0.2	8.436	8.171	0.3
T_CO2_HTR_p_low_side_in	°C	77.759	77.781	0.0	300.213	300.189	0.0	447.576	447.592	0.0

DOI: 10.17185/duepublico/48916

(1LKB42CT001)										
p_CO2_LTR_p_low_side_out (1LKB60CP001)	MPa	8.877	8.894	0.0	7.562	7.574	0.0	8.020	8.032	0.0
T_CO2_LTR_p_low_side_out (1LKB60CT001)	°C	42.177	43.981	-1.8	39.155	39.484	-0.3	37.825	39.390	-1.6

*Note that all pressures are gauge pressures.

ANNEX G
MEASSURED AND CALCULATED STEADY STATE PARAMETERS

parameter	Unit	step-Up_meass	step-Up	error_abs	step-Down_meass	step-Down	error_abs
m_CO2_MP (1LKB70CF001)	kg/s	0.001	0.000	0.0	0.001	0.132	-0.1
m_CO2_LTR (1LKB10CF001)	kg/s	0.131	0.132	0.0	0.131	0.132	0.0
power_H1/1 (1LKD40CE011A)	kW	3.116	3.821	-0.7	1.295	2.123	-0.8
power_H1/2 (1LKD40CE011B)	kW	3.169	3.821	-0.7	1.373	2.123	-0.7
power_H2 (1LKD40CE011C)	kW	6.206	6.128	0.1	10.901	11.200	-0.3
power_H3 (1LKD10CE011)	kW	15.381	14.131	1.2	14.705	13.247	1.5
p_CO2_MP_in (1LKB70CP001)	MPa	7.581	7.533	0.0	7.493	7.433	0.1
T_CO2_MP_in (1LKB70CT001)	°C	16.152	16.047	0.1	16.236	16.047	0.2
p_CO2_MP_out (1LKB10CP001)	MPa	10.346	10.457	-0.1	10.465	10.723	-0.3
T_CO2_MP_out (1LKB10CT001)	°C	17.663	19.454	-1.8	17.947	19.889	-1.9
position_valve_LTR_in (1LKB10CG001)	%	0.000	1.000	-1.0	0.000	1.000	-1.0
position_valve_LTR_by-pass (1LKB11CG001)	%	100.000	100.000	0.0	100.000	100.000	0.0
T_by-pass LTR (1LKB12CT001)	°C	44.978	45.000	0.0	45.000	45.000	0.0
p_CO2_LTR_p_high_side_in (1LKB10CP003)	MPa	10.359	10.416	-0.1	10.476	10.683	-0.2
T_CO2_HTR_p_high_side_out (1LKB30CT001)	°C	73.478	69.844	3.6	87.678	82.396	5.3
p_CO2_HTR_p_high_side_out (1LKB30CP001)	MPa	10.326	10.396	-0.1	10.450	10.662	-0.2
T_CO2_H1/1_H1/2_in (1LKD40CT001)	°C	73.506	69.684	3.8	87.697	82.229	5.5
T_CO2_H1/1_out (1LKD40CT002)	°C	100.030	100.000	0.0	100.015	100.002	0.0
T_CO2_H1/2_out (1LKD40CT003)	°C	100.032	100.000	0.0	100.009	100.002	0.0
T_CO2_H2_out (1LKD40CT004)	°C	130.007	130.000	0.0	156.473	157.108	-0.6
p_CO2_RV_in (1LKB31CP001)	MPa	10.333	10.320	0.0	10.453	10.579	-0.1
T_CO2_RV_in (1LKB31CT001)	°C	131.158	129.322	1.8	157.165	156.287	0.9
position of RV (1LKB31CG001)	%	100.029	100.029	0.0	100.029	100.029	0.0
position_valve_CH2_by-pass (1LKB40CG001)	%	99.337	99.337	0.0	99.617	99.617	0.0
p_CO2_HTR_p_low_side_in (1LKB42CP001)	MPa	7.768	7.649	0.1	7.684	7.549	0.1
T_CO2_HTR_p_low_side_in (1LKB42CT001)	°C	116.219	114.154	2.1	142.026	139.466	2.6
p_CO2_LTR_p_low_side_out (1LKB60CP001)	MPa	7.597	7.557	0.0	7.509	7.458	0.1
T_CO2_LTR_p_low_side_out (1LKB60CT001)	°C	43.855	43.218	0.6	43.919	43.302	0.6

*Note that all pressures are gauge pressures.

DOI: 10.17185/duepublico/48916

DOI: 10.17185/duepublico/48916
URN: urn:nbn:de:hbz:464-20191002-164705-5